IAHR AIRH

25th IAHR International Symposium on Ice
Trondheim, June 14 to 18, 2020

Elasticity and viscosity of ice measured in the experiment on wave propagation below the ice in HSVA ice tank

Aleksey Marchenko[1], Andrea Haase[2], Atle Jensen[3], Benjamin Lishman[4], Jean Rabault[3], Karl-Ulrich Evers[5], Mark Shortt[6], Torsten Thiel[7]

[1]*The University Centre in Svalbard*
PO Box 156, N-9171 Longyeabryen, Norway
Aleksey.Marchenko@unis.no
[2]*Arctic Technology, Hamburgische Schiffbau-Versuchsanstalt GmbH, Hamburg Ship Model Basin, Hamburg, Germany*
[3]*University of Oslo, Oslo, Norway*
[4]*London South Bank University, UK*
[5]*Solutions4arctic, Germany*
[6]*University College London, UK*
[7]*Advanced Optics Solutions GmbH, Germany*

An experiment on the propagation of flexural-gravity waves was performed in the HSVA ice tank in 2018. Physical characteristics of the water-ice system were measured in different locations in the tank during the tests, with several sensors deployed in the water, on the ice and in the air. Periodical waves with frequencies of 0.5-1.5 Hz were generated by HSVA wave maker during 10 min in each test. The phase speeds and wave damping associated with anelastic deformations of ice were analyzed in the paper. Elastic modulus of ice was calculated for each wave period from the dispersion equation of flexural gravity waves where measured values of wave frequencies and wave speeds were substituted. Viscous coefficient of ice was calculated after the analysis of wave damping. Obtained values have relatively big dispersion which can be explained by natural variability of ice properties.

1. Introduction

Sea ice coverage in the Arctic Ocean is decreasing. This leads to an increase in the probability of storms in ice-free areas (Sepp and Jaagus, 2011). Surface waves and swell penetrate from stormy regions of the ocean into ice-covered regions, and induce ice failure. The low frequency component of swell propagates across long distances under the ice without ice failure and with very little damping, causing bending oscillations of Arctic pack ice. Measurements of swell in Arctic pack ice have been made in the Beaufort Sea (Crary et al., 1952) and in the Central Arctic (Hunkins, 1962; LeSchack and Haubrich, 1964; Sytinskii and Tripol'nikov, 1964), using gravity-meters and seismometers. Recently, Mahoney et al., (2016) measured low frequency swell using short-temporal-baseline interferometric synthetic aperture radar. Hunkins (1962), Sytinskii and Tripol'nikov (1964), Gudkovich and Sytinskii (1965) and Smirnov (1996) measured waves with periods of 8-15s. These are associated with local processes in drift ice, caused by wind action on ice ridges, floe-floe interactions, etc. Physical mechanisms of wave damping in solid ice include viscous and anelastic bending deformations of ice, energy dissipation in the ice-adjacent boundary layer, and brine pumping (Marchenko and Cole, 2017; Rabault et al., 2020).

Wave actions on pack ice and land-fast ice are similar because both involve solid ice. The action of the land-fast ice on incoming waves is combined with the effects of bathymetry, shoreline and islands. These combined effects can lead to diffraction, refraction and reflection of waves, leading to waves with more complicated configurations. The amplitude of ocean swell in shallow water regions becomes higher, and the wavelength becomes shorter. This swell can also cause the breakup of land-fast ice near the shoreline. Zubov (1944) describes the breakup of landfast ice near Cape Chelyuskin and Tiksi Bay on 26th-28th January 1943 by large waves, despite the fact that the ice thickness throughout the Laptev Sea was greater than 1m. Bates and Shapiro (1980) recorded vertical displacements of ice with amplitude of several centimeters and with a period around 600s, prior to a significant ice push episode in land-fast sea ice (1.5-2m thick) near Point Barrow, Alaska. Further, over five years of near-continuous radar observations of near-shore ice motion in that area, similar oscillations were always observed to occur for several hours before the start of movement of land-fast ice or adjacent pack ice. Wave events were associated with momentum transfer from sea ice into the water during ice ridge buildup between land-fast ice and drift ice in the Beaufort Sea (Marchenko et al., 2002). The breakup of land-fast ice of 0.5m thickness, in shallow water near the shore in the Ice fjord of Spitsbergen, due to swell with period 7s and amplitude 10-15cm, is described by Marchenko et al. (2011). This work also shows that the maximum bending stresses in the ice during the breakup event were comparable to the flexural strength measured in the same place several days earlier. The action of a tsunami-wave on land fast ice (1m thick, near Tunabreen glacier in Temple Fjord, Spitsbergen) is described by Marchenko et al. (2013). The duration of the leading wave pulse was 40s, and the wave tail included waves with periods around 10s and 16s. Sutherland and Rabault (2015) investigated how swell penetrates from open water into land-fast ice (0.5m thick, in Temple Fjord, Spitsbergen), and were able to measure the attenuation of waves, with periods 4-10s, in the land-fast ice.

In 2015 and 2016, several tests on wave-ice interaction were performed at the Large Ice Model Basin (LIMB) of the Hamburg Ship Model Basin (Hamburgische Schiffbau-Versuchsanstalt, or HSVA) (Cheng et al, 2017; Tsarau et al., 2017; Hermans et al., 2018). The main goals of these tests were (1) to investigate the distribution of floe sizes when an initially continuous uniform ice sheet was broken by regular waves with prescribed characteristics, (2) to measure wave attenuation and dispersion in broken ice, and (3) to improve understanding of ice-structure interaction under wave conditions. Wave characteristics were reconstructed from the

records of water pressure sensors mounted on the tank wall. Tests were performed with wave lengths around 2.5m and 6.17m. Both ice breakup (starting from the ice edge) and wave attenuation were observed in the tests with wavelength around 2.5m.

In this paper we present some results of tests performed in January 2018 in the Large Ice Model Basin (LIMB) of HSVA. The work was supported by the Hydralab+ project "Investigation of bending rheology of floating saline ice and physical mechanisms of wave damping". The aims are to observe and describe physical processes in solid ice during wave propagation; to investigate the bending rheology; and to investigate the damping of waves propagating below solid ice. These aims are realized by performing a suite of measurements during wave propagation below solid ice. The present paper is structured as follows. Section 2 provides a description of the rheological viscous-elastic model of ice and gives formulas for the calculation of elastic and viscous characteristics of ice from the experimental data. Organizing of the experiment is described in Section 3. Collected experimental data are described and estimates of elastic and viscous ice constants are given in Section 4. Results of investigations are summarized and discussed in Conclusions (Section 5).

2. Dispersion and damping of surface waves propagating below thin viscous-elastic plate

Propagation of waves with small amplitudes in water layer covered by thin sold ice plate is investigated with using of the following model including the second order equation for the velocity potential φ (Greenhill, 1887):

$$\left(\frac{\partial^2}{\partial x^2}+\frac{\partial^2}{\partial z^2}\right)\varphi = 0,\ z \in (-H, 0), \qquad [1]$$

and boundary conditions and the bottom and below the ice plate

$$\frac{\partial \varphi}{\partial z} = 0,\ z = -H;\ \frac{\partial \eta}{\partial t} = \frac{\partial \varphi}{\partial z},\ z = 0;\ \frac{\partial \varphi}{\partial t} + g\eta = \frac{1}{\rho_w}\frac{\partial^2 M_{xx}}{\partial x^2},\ z = 0. \qquad [2]$$

Here η is the elevation of ice plate, M_{xx} is the bending moment in the ice plate, ρ_w and H are the water density and water depth, g is the gravity acceleration, t is the time, and x and z are the horizontal and vertical coordinates.

The bending moment and longitudinal strain are determined according classical theory of thin plates (Timoshenko and Woinowsky-Krieger, 1959)

$$M_{xx} = \int_{-h/2}^{h/2} \zeta \sigma_{xx} d\zeta,\ \varepsilon_{xx} = -\zeta \partial^2 \eta / \partial x^2, \qquad [3]$$

where σ_{xx} is the longitudinal stress caused by bending deformations of the ice, ζ is the transversal coordinate perpendicular to the middle surface of the plate, and h is the plate thickness.

Rheology of small viscous-elastic deformations of ice is descried by a linear combination of the Maxwell and Voight units described by the equation (Ashton, 1986)

$$\ddot{\varepsilon}_{xx} + \frac{E_2}{\eta_2}\dot{\varepsilon}_{xx} = \frac{1}{E_1}\ddot{\sigma}_{xx} + \left(\frac{1}{\eta_1}+\frac{1}{\eta_2}+\frac{E_2}{E_1\eta_2}\right)\dot{\sigma}_{xx} + \frac{E_2}{\eta_1\eta_2}\sigma_{xx}, \qquad [4]$$

where E_1 and E_2 are the elastic moduli, and η_1 and η_2 are the coefficients of viscosity. Dots and double dots above the symbols mean the first and the second derivatives with respect to the time.

Solution of equations [1] and [2] is expressed by the formula

$$\varphi = \varphi_0 e^{i\theta} \frac{\cosh[k(z+H)]}{\cosh[kH]}, \eta = ae^{i\theta}, \varphi_0 = i\omega a/(k\tanh[kH]), \theta = kx + \omega t, \quad [5]$$

where ω and k are the wave frequency and the wave number, and a is the wave amplitude. The wave frequency and the wave number satisfy to the dispersion equation

$$\frac{\omega^2}{k\tanh[kH]} = g + \frac{E_1 h^3 k^4}{12\rho_w} \frac{1 - iE_2/(\eta_2\omega)}{1 - \frac{iE_1}{\omega}\left(\frac{1}{\eta_1} + \frac{1}{\eta_2} + \frac{E_2}{E_1\eta_2}\right) - \frac{E_1 E_2}{\omega^2 \eta_1 \eta_2}}. \quad [6]$$

Wave damping is associated with the imaginary terms of equation [8]. These terms are small if wave damping occurs over a distance much greater than the wavelength. The imaginary terms are small when $E_1/\omega\eta_1 \ll 1$ and $E_2/\omega\eta_2 \ll 1$.

Now the dispersion equation can be approximated by the formulas

$$\omega = \omega_{fg}(1 + i\beta), \omega_{fg}^2 = k\tanh[kH]\left(g + \frac{E_1 h^3 k^4}{12\rho_w}\right), \beta = \frac{E_1 h^3 k^4}{24\rho_w (g + E_1 h^3 k^4/12\rho_w)} \frac{E_1}{\omega\mu}, \quad [7]$$
$$\mu = \eta_1\eta_2/(\eta_1 + \eta_2).$$

Spatial decay of the amplitude of a periodic wave is described by the equation (Caster, 1962)

$$\eta = \eta_0 e^{i\theta - \omega\beta c_g^{-1} x}, \quad [8]$$

where $c_g = \partial\omega_{fg}/\partial k$ is the wave group velocity. Further we consider the wave damping coefficient $\alpha = \omega\beta c_g^{-1}$.

Assuming that in the leading order the phase speed is determined by the formula $c = \omega_{fg}/k$, the elastic constant E_1 is calculated with the formula

$$E_1 = 12\rho_w (c^2 \coth[kH] - g)(k^4 h^3)^{-1}. \quad [9]$$

The viscous constant is calculated from formula [7] as follows

$$\mu = \frac{E_1^2 k^4 h^3}{24\alpha c_g \rho_w (g + E_1 h^3 k^4/12\rho_w)}. \quad [10]$$

3. Organizing of experiment

During the experiment in HSVA ice tank wave maker produced periodic waves propagating below solid ice with thickness of 5 cm. The tank width is 10 m, and the tank length is 70 m. Locations of sensors used in the experiments are pointed out in the frame of reference (x, y, z), where the origin is located at the right corner at the bottom of the tank near the wave maker. The ice sheet affects actual wave heights in the tank due to damping in the ice covered region (12 m < x < 62 m) and due to reflections from the ice edge in the region with open water (0 <

x < 12 m). Wave reflection from the end of the tank can be ignored in the tests because of the small wave amplitudes at the end of the tank and the relatively small wave lengths.

Waves characteristics were registered with fiber optics strain sensors (FBGS sensors), optical system Qualisys, Ultra Sonic sensors and water pressure (WP) sensors. FBGS sensor measured longitudinal strain of the fiber with working length of 20 cm mounted on the ice surface with two brackets each of which was screwed to the ice by four screws (Fig. 1a). Bending deformations of ice influenced the change of fiber tension with the wave period. FBGS sensors were installed in the longitudinal and transversal directions of the tank around $x = 20$ m (FBGS 1-4, Fig. 1b) and $x = 50$ m (FBGS 5-8), where x is the longitudinal coordinate extended along the ice tank axis. The tank width is 10 m, and the tank length is 70 m. The ice edge was located at $x = 12$ m. Distance between sensors FBGS1 and FBGS2 was about 63 cm. Similar distance was between sensors FBGS5 and FBGS6. Air, ice and water temperature was recorded by temperature strings FBGT1 and FBGT2 with spatial resolution of 1 cm. Sampling interval of FBGS and FBGT sensors was 40 Hz.

A Qualisys™ motion capture system is used to detect the rigid body motions of the ice in all six degrees of freedom (6-DOF). The system uses four cameras, installed on the main carriage, to detect markers which are located at different positions on the model. Figure 2 shows locations of 5 markers of the system placed on the ice around $x = 28$ m by a cross: one marker was in the middle, two markers oriented in the longitudinal direction of the tank, and two markers oriented in the transversal direction of the tank. Distances between the middle marker 2 and two markers 1 and 3 oriented along the tank axis were 1.547 m and 1.344 m. Qualisys provided records of the displacements of each marker in the directions x, y, and z with sampling frequency of 200 Hz. Waves influenced mainly vertical displacements of the markers, while their horizontal positions were similar during the tests.

Eight water pressure sensors (WP) were mounted on the tank wall at 30 cm depth below the ice (Fig. 3). They were located at $x = 8$ m (1 WP sensor in open water area), $x = 24$ m (3 WP sensors with 30 cm distance between them), and $x = 56$ m (3 WP sensors with 30 cm distance between them). Measurements were performed with sampling frequency of 200 Hz. Further the results of measurements with FBGS, Qualisys and WP sensors are discussed.

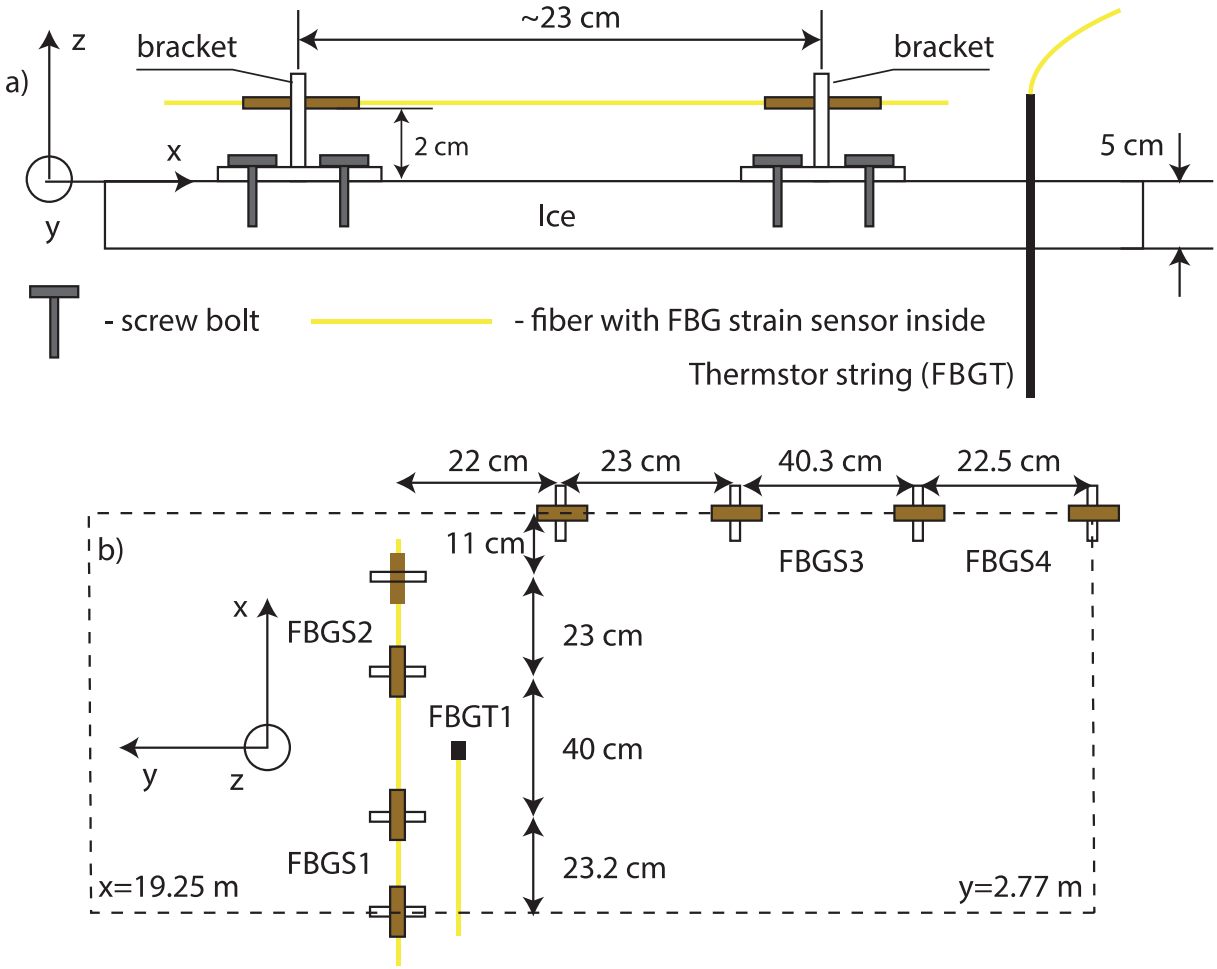

Figure 1. Mounting of the fibre optic strain sensor (FBGS) and temperature string (FBGT) on the ice (a). Spatial locations of FBGS 1-4 and FBGT sensors (b).

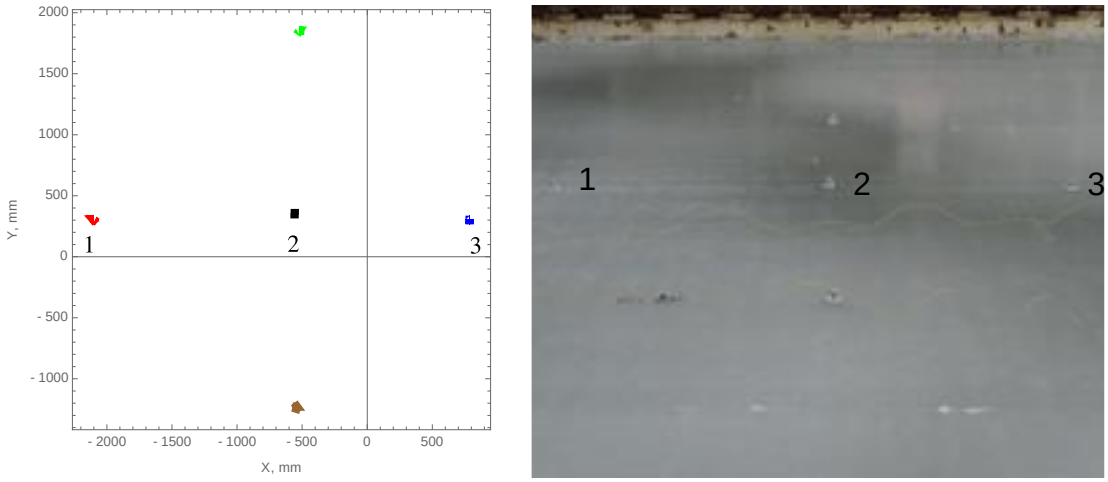

Figure 2. Locations of Qualisys markers in the local reference frame (left panel). Photographs of the markers on the ice. Markers 1, 2 and 3 are oriented along the tank axis. Marker 2 is located at $x = 28$ m.

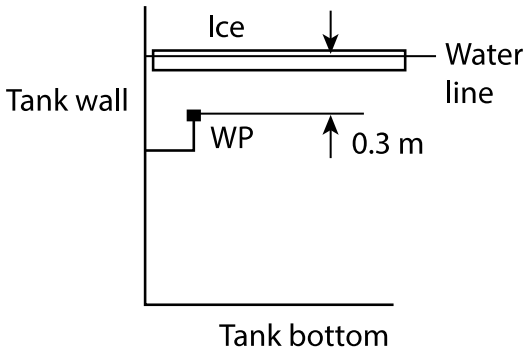

Figure 3. Mounting of the water pressure sensors at the tank wall.

4. Calculation of rheological constants

On the first stage the data were analysed to select time intervals were recorded amplitudes have relatively small dispersion. The duration of each test when the wave maker was programmed to generate periodic waves with prescribed height and frequency was 10 min. Usually the amplitudes of ice strains and vertical displacements changed in the beginning of each test during of approximately 50-100 sec, and then they became more stable. The dispersion of wave amplitudes was observed over each test, but in the beginning of the tests the amplitude dispersion was higher. All twelve tests disussed in the present paper were performed in one day of January 16. The ice temperature varied between -0.4C and -0.45C. The ice thickness was 5 cm. Wave height according to the wave maker setup was set to 5 mm in the first six tests and to 10 mm in the second six tests.

The analysis of phase speeds was performed for a fragment of each record with relatively small amplitude dispersion to minimize the influence of the modulations on the calculated phase speed. Time moments when strains recorded by FBGS 1-2, FBGS 5-6 reached local maxima were calculated for all performed tests. Time intervals Δt between local maxima recorded by FBGS1 and FBGS2 were used for the calculation of the phase speed of waves by the formula $c = L/\Delta t$, $L = 63$ cm. Similar calculations were performed with records of FBGS5 and FBGS6, and records of markers 1 and 2 and markers 2 and 3 of Qualisys system. Figure 4 shows phase velocities versus the wave frequency calculated with using of FBGS1-2 data (left panel) and Qualisys markers 1-2 (right panel). FBGS sensors showed a drop of the phase velocity to 2.8 m/s in two tests with wave frequency of 0.7 Hz, and an increase of the phase velocity to 3.6-3.8 m/s in two tests with wave frequency of 0.8 Hz. Qualisys data showed phase velocity in the range of 3.25-3.45 m/s in the tests with wave frequencies of 0.7 Hz and 0.8 Hz. In the most of the tests phase velocity is greater when the wave height is greater. Colored lines show analytical dependencies of the phase velocity from the wave frequency calculated with the formula $c = \omega_{fg}/k$ with three values of the elastic modulus $E_1 = 100, 150$ and 200 MPa.

Figure 5 shows elastic modulus versus the wave frequency calculated by formula (13) using the data of FBGS (left panel) and Qualisys system (right panel). Static point bending tests performed before and after the wave tests showed the values of elastic modulus of 88 MPa and 126 MPa respectively. Most of the whe wave tests showed higher values of elastic modules in the tests with bigger wave heights. The wave tests showed that the elastic modulus is around of 150 MPa or higher when the wave frequency was 0.9 Hz and 1 Hz. FBGS records showed that the elastic modulus is higher then 200 MPa in the tests with the wave frequency of 0.8 Hz, and it is of around 50 MPa in the tests with the wave frequency of 0.7 Hz. Qualisys data showed that elastic modulus varied between 110 MPa and 150 MPa in the tests with the wave frequency of 0.8 Hz, and between 130 MPa and 190 MPa in the tests with the wave frequency of 0.7 Hz.

The mean value of elastic modulus was around 120 MPa in the tests with the wave frequency of 0.5 Hz and 0.6 Hz according to FBGS data. Qualisys data showed similar values for these frequencies.

Figure 6 shows wave damping over 30 m distance according to the records of FBGS1 and FBGS5 sensors. One can see that damping of strains in stronger for higher wave frequencies. The wave damping coefficient can be calculated with the formula $\alpha = \log(a_1/a_2)/\Delta x$, where a_1 and a_2 are the strain amplitudes registered at different spatial locations, and $\Delta x = 30$ m is the distance between the locations. Then, the viscous constant is calculated from formula [10].

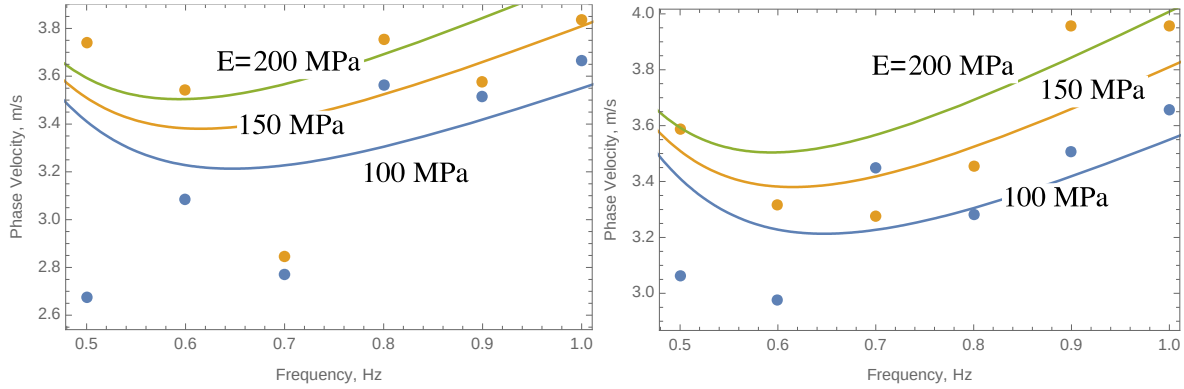

Figure 4. Phase velocities versus the wave frequency measured by FBGS sensors (left panel) and Qualisys system (right panel). Wave height according to the wave maker setup is 5 mm (blue points) and 10 mm (yellow points).

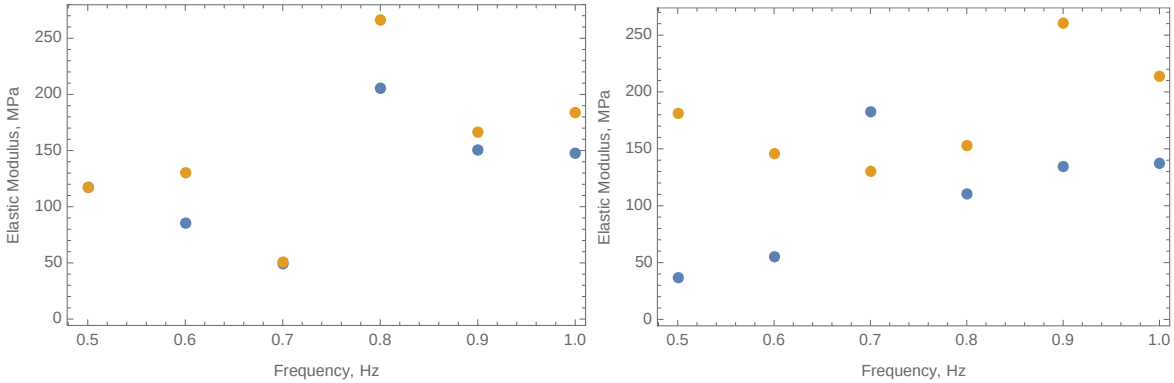

Figure 5. Elastic modulus versus the wave frequency measured by FBG strain sensors (left panel) and Qualisys system (right panel). Wave height according to the wave maker setup is 5 mm (blue points) and 10 mm (yellow points).

Figure 7 (left panel) shows the wave damping coefficient versus the wave frequency, and Fig. 7 (right panel) shows the viscous constant versus the wave frequency. The representative value of the viscous constant of ice is around $3 \cdot 10^8$ kg/(m s). Figure 8 (left panel) shows the dimensionless coefficient β specified in formula [7] versus the wave frequency. One can see that the approximation $\beta \ll 1$ is satisfied. The wave damping coefficient was calculated also from the data of WP sensors. The coefficient α was calculated using the absolute values of the discrete Fourier transforms of the WP data at the wave frequency. The values of a_1 and a_2 were equal to the discrete Fourier transforms applied to the records of WP sensors located at $x = 24$ m and $x = 56$ m. The results are shown in Fig. 8 (right panel). Left panel in Fig. 7 and left panel in Fig. 8 show that the wave damping coefficients calculated from FBGS data and WP sensors data are in the same range.

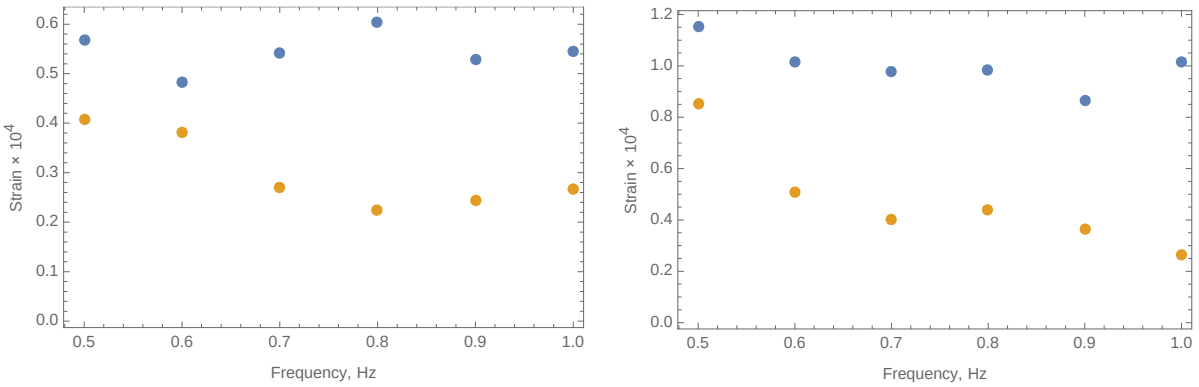

Figure 6. Longutudinal strains recorded by FBG strain sensors versus the wave frequency at the distances of 20 m (blue points) and 50 m (yellow points) from the beginning of the tank. Wave height according to the wave maker setup is 5 mm (left panel) and 10 mm (right panel).

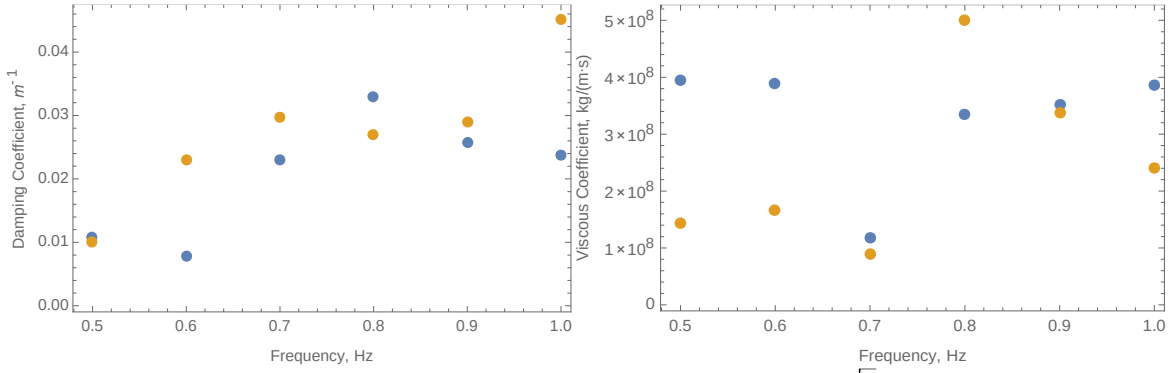

Figure 7. Damping coefficients (left panel) and viscous constant μ (right panel) versus the wave frequency reconstructed from the records of FBGS sensors. Wave height according to the wave maker setup is 5 mm (blue points) and 10 mm (yellow points).

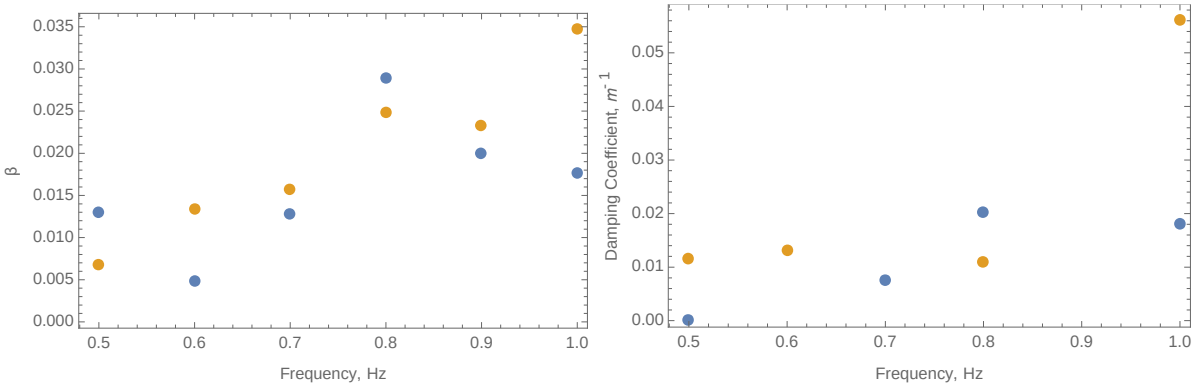

Figure 8. The dimensional coefficient β calculated with FBGS data (left panel) and the damping coefficient calculated with the records of the water pressure sensors versus the wave frequency. Wave height according to the wave maker setup is 5 mm (blue points) and 10 mm (yellow points).

5. Conclusions

Data of twelve tests on the propagation of flexural-gravity waves below solid ice with 5 cm thickness were processed and analyzed. The ice temperature during these tests was almost constant. Wave frequency changed in the tests from 0.5 Hz to 1.0 Hz with the step of 0.1 Hz. Wave maker was programmed to produce waves with amplitudes 5 mm in the first six tests,

and 10 mm in the other 6 tests. Duration of each test was 10 min. Because of small wave amplitudes we assumed that creep behavior of ice is described by liear model (Schulson and Duval, 2009). Linear comination of the Mawell and Voight units was used to describe ice rheology under bending deformations.

Analysis of wave characteristics showed an increase of the elastic modulus of model ice with the wave frequency. Data of FBGS sensors showed maximal values of the elastic modulus up to 250 MPa for the waves of 0.8 Hz frequency. Qualisys records showed maximal values of the elastic modulus up to 250 MPa for the waves with the frequency of 0.9 Hz. The elastic moduli were higher in the tests with higher wave amplitudes. Minimal value of the elastic modulus of 50 MPa was obtained from FBGS data from the tests with the wave frequency of 0.7 Hz. Qualisys data showed minimal values of the elastic modulus of around 50 MPa in the tests with the wave frequincies of 0.5 Hz and 0.6 Hz. The elastic moduli measured from the tests with the wave frequencies of 0.8 Hz, 0.9 Hz and 1.0 Hz were higher than elastic moduli determined from quasi-static tests on point bending: 88 MPa (before the tests) and 126 MPa (after the tests). Nine values of the phase speed calculated from the Qualisys records in the twelve tests are located within theoretical dependencies of the phase speed of flexural-gravity waves constructed with the elastic moduli of 100 MPa and 200 MPa. FBGS data showed stronger dispersion of the phase speeds.

FBGS data showed wave damping over 30 m distance. The viscous ice constant derived from these data varied between 10^8 kg/(m s) and $5 \cdot 10^8$ kg/(m s). Tabata (1958) and Lindgren (1968) estimated the viscous coefficient in the Voight unit of 10^{13} kg/(m s) (sea ice at -10 C) and $(6 \div 43) \cdot 10^{10}$ kg/(m s) (fresh ice at -5C ÷ -2.3C). The damping coefficient increased from 0.01 m^{-1} to 0.05 m^{-1} when the wave frequency increased from 0.5 Hz to 1.0 Hz. Water pressure records showed similar values of the wave damping coefficient. The dimensionless coefficient β calculated with FBGS data was smaller than 0.036, i.e. the approximation $\beta \ll 1$ used to simplify the dispersion equation was satisfied in the all tests.

Acknowledgments
The work was supported by the Research Council of Norway through the Petromks-2 project Dynamics of Floating Ice and IntPart project Arctic Offshore and Coastal Engineering in Changing Climate.

References

Ashton, G.D. (Editor), 1986. River and Lake Ice Engineering. Water Resources Publications. Michigan.

Bates, H., F., Shapiro, L.H., 1980. Long-period gravity waves in ice-covered sea. J. Geoph. Res., 85(2), 1095-1100.

Caster, M., 1962. A note on the relation between temporally-increasing and spatially-increasing disturbances in hydrodynamic instability. J. Fluid Mech., 14, 222-224.

Cheng, S., Tsarau, A., Li, H., Herman, A., Evers, K.-U., Shen, H., 2017. Loads on Structure and Waves in Ice (LS-WICE) Project, Part 1: Wave Attenuation and Dispersion in Broken Ice Fields. POAC17-046.

Greenhill, A.G., 1887. Wave motion in hydrodynamics. Am. J. Math., 9: 62-112.

Crary, A. P., Cotell, R. D. and Oliver, J. (1952). Geophysical studies in the Beaufort Sea, 1951. Transactions of the American Geophysical Union, Vol. 33, No. 2, p. 211–16.

Hermans, A., Evers, K.-U., Reimer, N., 2018. Floe-size distribution in laboratory ice broken by waves. The Cryosphere, 12, 685-699.

Hunkins, K., 1962. Waves in the Arctic Ocean. J. Geoph. Res., 67(6), 2477-2489.

Gudkovich, Z.M., Sytinskii, A.D., 1965. Some observation results of tidal phenomena in Arctic basin using tilt-meters. Okeanologia, 5(5), 75-85. (in Russian)

LeSchack, L.A., Haubrich, R.A., 1964. Observations of waves on an ice-covered ocean. J. Geoph. Res., 69(18), 3815-3821.

Lindgren, S., 1968. Effect of temperature increase o ice pressure. Institute of Hydraulic Engineering, Royal Institute of Technology, Stockholm.

Marchenko, A., Makshtas, A., Shapiro, L., 2002. On the excitation of shelf-edge waves due to self-induced oscillations of ice floes. In: Squire, V. A. and P. J. Langhorne (Eds), Ice in the Environment: Proc. 16th Intern. Symp. on Ice, vol. 2. Intern. Assoc. Hydraulic Eng. & Res., Dunedin, New Zealand, 301-309.

Marchenko, A., Shestov, A., Karulin, A., Morozov, E., Karulina, M., Bogorodsky, P., Muzylev, S., Onishchenko, D., Makshtas, A., 2011. Field studies of sea water and ice properties in Svalbard fjords. POAC11-148.

Marchenko, A.V., Morozov, E.G., Muzylev, S.V., 2013. Measurements of sea-ice flexural stiffness by pressure characteristics of flexural-gravity waves. Annals of Glaciology, 54(64), 51-60.

Marchenko, A., Cole, D., 2017. Three physical mechanisms of wave energy dissipation in solid ice. POAC17-086.

Rabault, J., Sutherland, G., Jensen, A., Christensen, K.H., Marchenko, A., 2019. Experiments on wave propagation in grease ice: combined wave gauges and particle image velocimetry measurements. J. Fluid Mech., 864, 876-898.

Schulson, E.M., Duval, P., 2009. Creep and fracture of ice. Cambridge University Press. 417 pp.

Sepp, M., Jaagus, J., 2011. Changes in the activity and tracks of Arctic cyclones, Clim. Change, 105(3–4), 577–595.

Smirnov, V.N., 1996. Dynamics processes in sea ice. St.-Petersburg, Gidrometeoizdat, 162 pp. (in Russian)

Sytinskii, A.D., Tripol'nikov, V.P., 1964. Some investigation results of natural oscillations of ice fields in Central Arctic. Izvestia AN SSSR. Geofizika. N4, 210-212. (in Russian)

Sutherland, G., Rabault, J., 2015. Observations of wave dispersion and attenuation in land fast ice. J. Geoph. Res. Oceans, 121, 1984-1987.

Tabata, T., 1958. Studies on visco-elastic properties of sea ice in Arctic Sea Ice, Arctic Sea Ice Conference, Easton, Maryland, 1958.

Timoshenko, S., Woinowsky-Krieger, S., 1959. Theory of plates and shells. 2nd ed., McGraw/Hill, New York, USA.

Tsarau, A., Sukhorukov, S., Herman, A., Evers, K.-U., Løset, S., 2017b. Loads on Structure and Waves in Ice (LS-WICE) project, Part 3: Ice-structure interaction under wave conditions, POAC17–068.

Zubov, N. N., 1943: Arctic Ice. Izdatel'stvo Glavsevmorputi, 360 pp. (English translation, AD 426 972, U.S. Nav. Oceanogr. Office, NTIS, 5285 Port Royal Rd., Springfield, VA 22161)